Communication in Physical Sciences, 2025, 12(8):2253-2270

Synthesis of Fe_3O_4 Nanoparticles Using Lichen (*Collema* ABU01502) Extract and their Application in the Removal of 4-Nitrophenol from Aqueous Solution

Ahmad Ahmad, Kehinde Israel Omoniyi, Nwokem Nsidibeabasi Calvin, Hamisu Ibrahim, Shuaibu Musa, and Ugwoke Augustina Oyibo

Received:24 October 2025/Accepted: 09 December 2025/Published: 13 December 2025
https://dx.doi.org/10.4314/cps.v12i8.7

~~**Abstract**~~: *In this study, magnetite (Fe_3O_4) nanoparticles were successfully synthesized via a green and sustainable route using Collema lichen (ABU01502) extract as a natural reducing and capping agent, and their application in the removal of 4-nitrophenol (4-NP) from aqueous solution was systematically investigated. Fourier Transform Infrared (FTIR) spectroscopy confirmed the presence of bio-derived functional groups (–OH, C=O, C–O, and aromatic moieties) on the nanoparticle surface alongside the characteristic Fe–O vibration around 580 cm^{-1}, indicating successful formation of magnetite with biomolecular capping. SEM and TEM analyses revealed quasi-spherical nanoparticles with partial agglomeration and particle sizes ranging from 10.0 to 28.5 nm. UV–Vis spectroscopy showed a broad absorbance between 300 and 800 nm, consistent with the optical behavior of Fe_3O_4 nanoparticles. Batch adsorption experiments demonstrated that 4-NP removal efficiency strongly depended on pH, temperature, contact time, and adsorbent dosage, with removal efficiencies ranging from approximately 4 % to 55 % prior to optimization. Response Surface Methodology (RSM) based on a 2^4 factorial design yielded a highly significant predictive model ($F = 37.10$, $p = 0.0063$) with a high coefficient of determination ($R^2 = 0.9933$). Optimal conditions (pH 8.0, 60 °C, 180 min, and 4 g L^{-1} adsorbent dosage) resulted in a maximum 4-NP removal of 74.93 % and a desirability of 1.0. Adsorption equilibrium was best described by the Langmuir isotherm ($R^2 = 0.9942$), with a monolayer adsorption capacity of 49.75 mg g^{-1} and a favorable separation factor ($R^L = 0.095$). These findings demonstrate that lichen-mediated Fe_3O_4 nanoparticles are efficient, magnetically recoverable, and environmentally benign adsorbents for nitrophenol-contaminated water treatment.*

Keywords: *Adsorption analysis, iron oxide nanoparticles, lichen extract, P-nitrophenol,*

Ahmad Ahmad
School of Basic and Remedial Studies, Ahmadu Bello University, PMB 06, Zaria 810211, Nigeria
Email: ahmadahmad9070@gmail.com
https://orcid.org/0009-0003-6484-3103

Kehinde Israel Omoniyi
Department of Chemistry, Ahmadu Bello University, P.M.B. 06, Zaria 810211, Nigeria
Email: israelflourish@yahoo.com
https://orcid.org/0009-0005-3224-9382

Nwokem Nsidibeabasi Calvin
Department of Chemistry, Ahmadu Bello University, PMB 06, Zaria 810211, Nigeria
Email: nsidibe19@gmail.com
https://orcid.org/0000-0001-7144-2111

Hamisu Ibrahim
Department of Chemistry, Ahmadu Bello University, PMB 06, Zaria 810211, Nigeria
Email: hamisuibrahim@abu.edu.ng
http://orcid.org/0000-0003-3022-7671

Shuaibu Musa
Department of Chemistry, Ahmadu Bello University, PMB 06, Zaria 810211, Nigeria
Email: shuaibupolymer@gmail.com
https://orcid.org/0009-0007-6807-5817

Ugwoke Augustina Oyibo
Department of Chemistry, Nigeria Police

Academy, Wudil, Kano State, P.M.B. 3474, Kano 713105, Nigeria
Email: augustinaaroh@yahoo.com
https://orcid.org/0009-0005-2668-2788

1.0 Introduction

Water pollution resulting from rapid industrialization and urban expansion has become a critical global environmental concern, posing severe threats to ecosystems and public health. Industrial effluents frequently contain toxic organic contaminants such as nitrophenols, dyes, pharmaceuticals, and persistent organic pollutants, which are resistant to natural degradation processes and accumulate in aquatic systems (Das et al., 2021). Among these contaminants, 4-nitrophenol (4-NP) is particularly hazardous due to its extensive use in the manufacture of pesticides, dyes, pharmaceuticals, petrochemicals, and leather-processing chemicals. Its high solubility, chemical stability, and nitro-substituted aromatic structure contribute to its persistence in water bodies and soils, making remediation difficult (Abdelfatah et al., 2021). Exposure to 4-NP has been linked to adverse health effects including liver and kidney damage, neurological disorders, ocular irritation, and systemic toxicity (Dhorabe et al., 2016; Benmaati et al., 2022). Consequently, the development of efficient, sustainable, and cost-effective treatment technologies for 4-NP-contaminated water is of paramount importance.

Conventional remediation methods such as membrane filtration, coagulation–flocculation, ion exchange, electrochemical treatment, and biological degradation have been employed for nitrophenol removal; however, many of these approaches suffer from drawbacks including high operational costs, secondary pollution, energy intensiveness, and limited efficiency for recalcitrant pollutants (Li et al., 2022; Tran et al., 2023). Adsorption-based techniques have emerged as one of the most promising alternatives due to their simplicity, high removal efficiency, low energy demand, and operational flexibility (Zhao et al., 2019). In recent years, nanostructured adsorbents and catalysts have attracted significant attention because of their high surface area, tunable surface chemistry, and enhanced reactivity.

Among engineered nanomaterials, magnetite (Fe_3O_4) nanoparticles have demonstrated exceptional potential for wastewater treatment applications. Their superparamagnetic behavior allows for rapid separation and recovery from aqueous systems using an external magnetic field, thereby facilitating reuse and minimizing secondary contamination (Shen et al., 2021). Fe_3O_4 nanoparticles exhibit strong adsorption affinity and catalytic activity toward organic pollutants, including nitroaromatic compounds, dyes, and phenols (Trujillo Hernandez et al., 2022). Furthermore, Fe_3O_4-based systems have been successfully employed in catalytic reduction processes, particularly in the transformation of 4-NP to the less toxic and industrially valuable 4-aminophenol in the presence of reducing agents (Vu et al., 2023).

Despite these advantages, conventional synthesis routes for Fe_3O_4 nanoparticles often involve toxic chemicals, harsh reaction conditions, and high energy consumption, raising environmental and safety concerns (Shen et al., 2021). To overcome these limitations, green synthesis strategies utilizing biological resources have gained considerable interest. Plant extracts, agricultural wastes, fungi, and other bio-resources have been shown to act as reducing, stabilizing, and capping agents during nanoparticle formation, enabling environmentally benign synthesis under mild conditions (Azizi et al., 2020; Bassim et al., 2022). Phytochemicals such as flavonoids, polyphenols, terpenoids, and polysaccharides play a crucial role in controlling particle size, morphology, and stability (Khatun et al., 2022). Numerous studies have reported successful green synthesis of Fe_3O_4 nanoparticles using plant-based extracts and their applications in wastewater treatment. For example, Bassim et

al. (2022) synthesized Fe_3O_4 nanoparticles using *Citrus aurantium* extract and achieved over 93% removal of methylene blue through adsorption optimized by response surface methodology. Similarly, Alamier et al. (2022) reported biogenic synthesis of Fe^0/Fe_3O_4 nanoparticles using *Caralluma acutangula* extract, demonstrating high catalytic efficiency for dye degradation under UV irradiation. Golabiazar (2023) and Khatun et al. (2022) further highlighted the antimicrobial and catalytic properties of phytochemically synthesized Fe_3O_4 nanoparticles with particle sizes below 15 nm. These studies confirm that green synthesis routes can produce highly functional Fe_3O_4 nanomaterials suitable for environmental applications.

More recently, researchers have explored composite and multifunctional Fe_3O_4-based materials for enhanced performance. Azizi et al. (2020) developed Fe_3O_4/cellulose nanocomposites with improved thermal stability and magnetic properties for biomedical applications, while Vu et al. (2023) demonstrated rapid catalytic reduction of 4-NP using Ag/Fe_3O_4/cellulose nanocomposites. Although these studies underscore the versatility of Fe_3O_4 nanoparticles, they often rely on plant extracts or synthetic supports, with limited attention given to alternative biological sources such as lichens.

Lichens are symbiotic organisms composed of fungi and algae, rich in unique secondary metabolites, polysaccharides, and phenolic compounds that can act as natural reducing and capping agents. Their resilience and biochemical diversity make them promising yet underexplored candidates for nanoparticle biosynthesis. Despite increasing reports on plant-mediated Fe_3O_4 synthesis, there remains a significant knowledge gap regarding the use of lichen extracts—particularly *Collema* species—in controlling nanoparticle nucleation, morphology, and adsorption performance toward nitrophenolic pollutants. Furthermore, systematic optimization of adsorption conditions for 4-NP removal using lichen-derived Fe_3O_4 nanoparticles remains scarcely reported.

Therefore, the aim of this study is to synthesize Fe_3O_4 nanoparticles via an environmentally friendly route using *Collema* lichen extract, characterize their structural, morphological, and functional properties, and evaluate their efficiency in the removal of 4-nitrophenol from aqueous solution. The adsorption process is further optimized using response surface methodology and isotherm modeling to elucidate the interaction mechanisms between the nanoparticles and the pollutant. The significance of this research lies in introducing a novel lichen-mediated green synthesis approach, advancing sustainable nanomaterial development, and providing an effective, magnetically recoverable adsorbent for the remediation of hazardous nitrophenolic contaminants in water systems.

2.0 Materials and Methods

2.1 Materials

Fresh lichen samples, ferric chloride hexahydrate ($FeCl_3 \cdot 6H_2O$), ferrous sulfate heptahydrate ($FeSO_4 \cdot 7H_2O$), sodium hydroxide (NaOH), deionized water, ethanol, and 4-nitrophenol were used in this study. All chemical reagents were of analytical grade and were purchased from Sigma-Aldrich and Thermo Fisher Scientific. The reagents were used as received without further purification.

The lichen extract was prepared by thoroughly cleaning the collected samples, scraping the lichen material from tree bark, and pulverizing it into a fine powder. Fifty grams of the powdered lichen were extracted in deionized water, and the resulting mixture was filtered using Whatman No. 1 filter paper. The filtrate was subsequently stored at 4 °C until further use.

2.2 Methods

2.2.1 Collection and Preparation of Lichen Extract

Fresh Collema sp. lichen samples were collected from bushes around Zaria, Nigeria. The collected samples were authenticated at the Department of Biological Sciences, Ahmadu Bello University, Zaria. The authenticated samples were washed thoroughly with deionized water to remove debris and impurities, air-dried, and processed as described in Section 2.1 for extract preparation.

2.2.2 Morphological and Structural Characterization

The structural and morphological properties of the synthesized Fe_3O_4 nanoparticles were characterized using Fourier Transform Infrared Spectroscopy (FTIR), Scanning Electron Microscopy coupled with Energy-Dispersive X-ray spectroscopy (SEM/EDX), and Transmission Electron Microscopy (TEM). Batch adsorption experiments were conducted to evaluate the removal efficiency of 4-nitrophenol using the synthesized nanoparticles. Response Surface Methodology (RSM) based on a Central Composite Design (CCD) was employed to optimize the adsorption process. Four independent variables (A–D) were studied at three coded levels (−1, 0, and +1), and the experimental runs were generated using Design-Expert software. Analysis of variance (ANOVA) was performed to determine the significance of the model, individual factors, and their interactions.

Adsorption equilibrium data were analyzed using Langmuir, Freundlich, and Temkin isotherm models, expressed in equations 1 to 3, respectively (Eddy *et al*., 2023)

$$\frac{C_e}{q_e} = \frac{C_e}{Q_0} + \frac{1}{bQ_0} \quad (1)$$

$$lnq_e = lnk_F + \frac{1}{n} lnC_e \quad (2)$$

$$q_e = \beta lnk_T + \beta lnC_e \quad (3)$$

Ce is the equilibrium concentration of the adsorbate in solution (mg L^{-1}), q_e is the amount of adsorbate adsorbed per unit mass of adsorbent at equilibrium (mg g^{-1}), Q_0 is the maximum monolayer adsorption capacity of the adsorbent (mg g^{-1}), b is the Langmuir adsorption constant related to the affinity between the adsorbent and adsorbate (L mg^{-1}), k_F is the Freundlich adsorption capacity constant indicative of adsorption strength, nnn is the Freundlich intensity parameter describing adsorption favorability, k_T is the Temkin isotherm equilibrium binding constant, and β\betaβ is the Temkin constant related to the heat of adsorption.

Data analysis was performed using Microsoft Excel for basic calculations, Design-Expert software for RSM analysis, and graphic representations. Results were presented as mean ± standard deviation, with significance set at $p < 0.05$.The TEM analysis was performed using a JEOL JEM-2100 microscope operating at 200 kV. Samples were prepared by dispersing Fe_3O_4 nanoparticles in ethanol and placing a drop on a carbon-coated copper grid. The images revealed well-dispersed spherical nanoparticles with sizes ranging from 10–30 nm. High-resolution TEM (HRTEM) showed clear lattice fringes, confirming crystallinity and phase purity. Selected Area Electron Diffraction (SAED) patterns matched the inverse spinel structure of Fe_3O_4, consistent with XRD results (Nguyen *et al.,* 2021). The Response Surface Methodology (RSM) based on Central Composite Design (CCD) was employed to optimize the adsorption conditions via Four independent variables (A-D) at three coded levels (-1, 0, +1), experimental runs generated by Design-Expert software. While the analysis of Variance (ANOVA) was conducted to identify significant factors and interactions.

3. 0 Results and Discussion

3.1 Fourier Transform Infrared (FTIR) Analysis

The FTIR spectrum of the green-synthesized Fe_3O_4 nanoparticles (Fig. 1) provides clear evidence of the involvement of *Collema* sp. lichen extract in nanoparticle formation and stabilization, as well as the successful formation of magnetite. Similar observations have been

widely reported for plant- and lichen-mediated synthesis of iron oxide nanoparticles, where phytochemicals act as both reducing and capping agents (Iravani, 2011; Ahmed et al., 2016).

A broad absorption band spanning 3235.3–3852.8 cm^{-1}, with notable features around 3652.8 cm^{-1} and 3757.2 cm^{-1}, is attributed to O–H stretching vibrations of hydroxyl groups present in phenolic compounds, cellulose, and carboxylic acids from the lichen extract. The broadness of this band indicates extensive hydrogen bonding, which is characteristic of biomolecule-assisted synthesis routes (Mittal et al., 2013; Singh et al., 2018). Hydroxyl groups have been reported to play a key role in reducing Fe^{3+}/Fe^{2+} ions and stabilizing the nanoparticle surface through coordination interactions (Prasad et al., 2017).

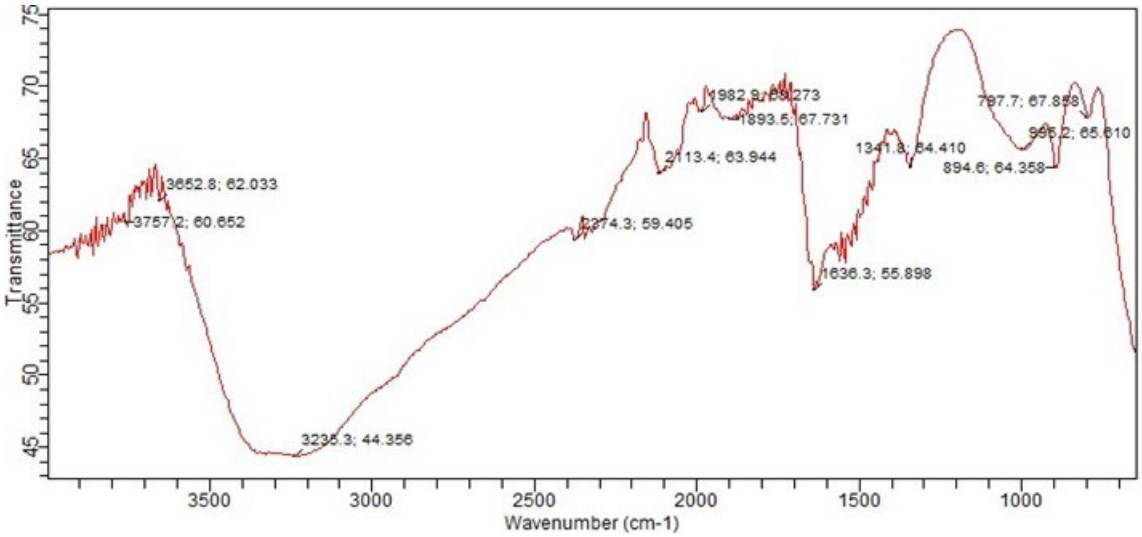

Fig. 1: FTIR spectra of the prepared Green Fe_3O_4

3.1 Furrier Transform Infrared (FTIR)

The absorption band near 3235.3 cm^{-1} corresponds to strongly hydrogen-bonded O–H stretching, while the peak observed at approximately 3757.2 cm^{-1} is associated with surface hydroxyl groups weakly bonded to iron atoms. Similar surface-bound hydroxyl vibrations have been reported for green-synthesized Fe_3O_4 nanoparticles and are indicative of surface functionalization, which enhances colloidal stability and adsorption capacity (Rai et al., 2015; Sahu et al., 2020).

The band observed at 1638.3 cm^{-1} is assigned to C=O stretching vibrations of carboxylate or amide groups, while the absorption at 1341.8 cm^{-1} corresponds to O–H bending and C–H bending vibrations of phenolic and aliphatic groups. These functional groups originate from secondary metabolites of the lichen extract and have been reported as major contributors to nanoparticle capping in biologically synthesized metal oxides (Kumar et al., 2014; Sharma et al., 2019). The presence of carboxyl and phenolic groups suggests strong surface binding and provides active sites for adsorption processes.

Weak absorption bands appearing between 2374.3 and 2113.4 cm^{-1} are attributed to C–N stretching and CH_2 bending vibrations, which may arise from nitrogen-containing biomolecules such as proteins or amino acid derivatives present in the lichen extract. Similar weak bands in this region have been reported for bio-capped Fe_3O_4 nanoparticles and are commonly associated with residual organic compounds from biological extracts (El-Shahawy et al., 2017; Abdallah et al., 2021).

The bands detected in the range of 995.2–797.7 cm^{-1} are assigned to aromatic C=C stretching vibrations, confirming the presence of aromatic rings derived from lichen secondary metabolites. Aromatic phytochemicals have been shown to contribute to nanoparticle stabilization and to enhance adsorption through π–π interactions with aromatic pollutants such as 4-nitrophenol (Wang et al., 2016; Mohan et al., 2020). Most importantly, the characteristic Fe–O stretching vibrations of magnetite are observed in the low-wavenumber region, typically around 575–580 cm^{-1}, which is diagnostic of the inverse spinel structure of Fe_3O_4. The appearance of this band confirms the successful formation of magnetite nanoparticles and is consistent with previous reports on both chemically and biologically synthesized Fe_3O_4 nanoparticles (Cornell and Schwertmann, 2003; Laurent et al., 2008).

Overall, the FTIR analysis confirms that the *Collema* sp. lichen extract effectively mediated the synthesis of Fe_3O_4 nanoparticles and contributed surface-bound hydroxyl, carboxyl, phenolic, and aromatic functional groups. These bio-derived functional groups are known to enhance adsorption performance through hydrogen bonding, electrostatic interactions, and π–π interactions, thereby improving the efficiency of Fe_3O_4 nanoparticles for the removal of organic contaminants such as 4-nitrophenol from aqueous systems (Foo and Hameed, 2010; Gupta et al., 2019).

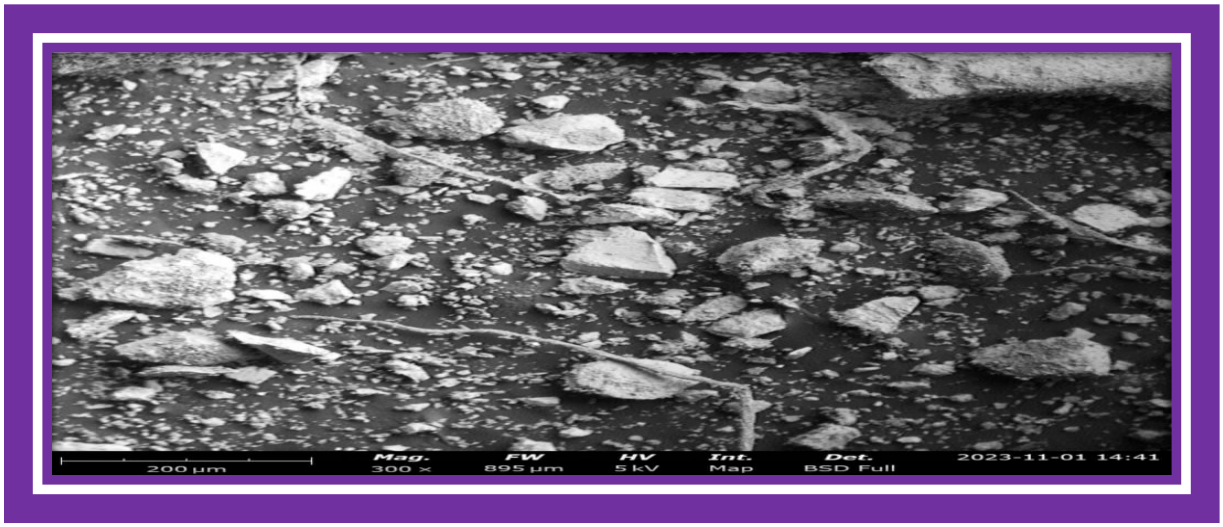

Plate 1: SEM Image of the prepared Fe_3O_4 at 200 μm

3.2 Scanning Electron Microscopy (SEM)

The SEM image of the prepared Fe_3O_4 nanoparticles presented in Plate 1 reveals an agglomerated morphology composed of irregularly shaped clusters distributed over the surface. The particles appear as coarse aggregates rather than isolated grains, which is characteristic of iron oxide nanoparticles synthesized via green routes, where magnetic interactions and surface-bound organic molecules promote particle clustering. The rough and heterogeneous surface texture observed suggests successful nucleation and growth of Fe_3O_4 nanoparticles mediated by lichen-derived phytochemicals.

Elemental composition analysis using SEM coupled with Energy Dispersive Spectroscopy (SEM–EDS) further confirms the formation of Fe_3O_4 nanoparticles. The dominant elements detected include iron (Fe, 26.27 %) and oxygen (O, 21.44 %), which collectively validate the presence of iron oxide as the primary phase. The substantial iron–oxygen composition is

consistent with previous reports on biosynthesized magnetite nanoparticles (Shaikh et al., 2022). The relatively high titanium (Ti, 34.48 %) content may be attributed either to environmental uptake of titanium from Ti-rich soils by the lichen or to the co-synthesis of TiO_2 nanoparticles arising from precursor impurities or biological accumulation, a phenomenon previously reported in plant-mediated nanoparticle synthesis (Alghamdi et al., 2023).

Trace elements such as carbon (C), silicon (Si), bromine (Br), tellurium (Te), and promethium (Pm) were also detected in minor amounts. Carbon (0.18 %) is indicative of residual organic compounds originating from lichen phytochemicals adsorbed onto the nanoparticle surface, which can enhance colloidal stability and biocompatibility, particularly for environmental and biomedical applications (Shaikh et al., 2022). The presence of Si, Br, and Te may result from inherent mineral constituents of the biological material or remnants from the extraction and synthesis processes. These trace elements can potentially influence the electronic structure, band gap, and photocatalytic behavior of the nanoparticles, which is increasingly exploited in multifunctional oxide nanocomposites (Jahan et al., 2021). Overall, the SEM and SEM–EDS results confirm the successful green synthesis of Fe_3O_4 nanoparticles with nanoscale features, surface functionalization, and complex elemental composition, although some degree of aggregation and trace-element incorporation remains a challenge.

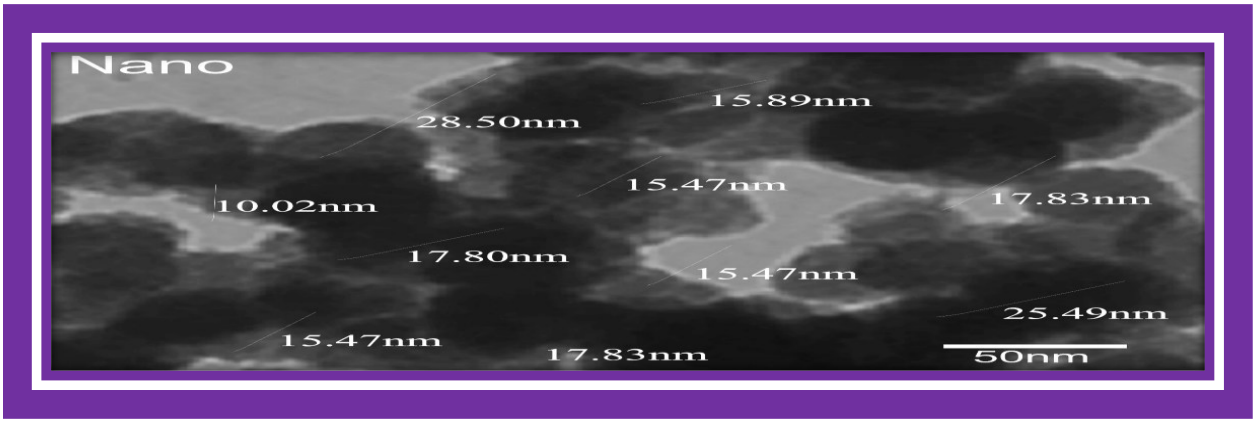

Plate 2: TEM Image of the prepared Green Fe_3O_4 at 200 μm

3.3 Transmission Scanning Microscopy

The TEM image of the biosynthesized Fe_3O_4 nanoparticles shown in Plate 2 provides detailed insight into particle morphology and size distribution. The nanoparticles are predominantly quasi-spherical in shape with relatively smooth edges, indicating controlled growth during synthesis. The measured particle sizes range from 10.02 nm to 28.50 nm, with a majority of particles falling within the 15.47–17.83 nm range, suggesting a narrow and dominant mid-nanoscale size distribution. This nanoscale dimensionality confirms the effectiveness of the green synthesis approach in producing fine magnetite nanoparticles (<30 nm). The relatively uniform morphology and size distribution can be attributed to the role of lichen-derived phytochemicals, such as polyphenols, flavonoids, and other bioactive compounds, which act as reducing, stabilizing, and capping agents during nanoparticle formation. These biomolecules regulate nucleation and growth processes, thereby preventing excessive particle enlargement and uncontrolled agglomeration, in agreement with earlier studies on plant-mediated synthesis of

metal oxide nanoparticles (Devi et al., 2021; Gao et al., 2022).

However, the TEM image also reveals partial clustering of nanoparticles, which is typical for iron oxide systems due to strong magnetic dipole–dipole interactions and hydrogen bonding between surface functional groups. While aggregation may reduce the available specific surface area, it can be advantageous for applications such as magnetic separation, adsorption, and catalysis, where collective magnetic behavior enhances performance (Chakraborty et al., 2023).

Taken together, the SEM and TEM analyses confirm the successful green synthesis of Fe_3O_4 nanoparticles with quasi-spherical morphology, nanoscale size distribution, and surface functionalization derived from lichen extract. The results further highlight the benefits of green synthesis routes, including sustainability, biocompatibility, and surface-modified nanoparticles, while also emphasizing the need for improved control over aggregation and trace-element incorporation for advanced applications such as photocatalysis, sensing, and magnetic remediation (Umar et al., 2024).

3.4 UV-Vis

UV–Vis spectrophotometry provided additional confirmation of nanoparticle formation. The lichen extract alone showed no distinct absorption peak in the visible region, indicating the absence of chromophoric species capable of strong light absorption. In contrast, the Fe_3O_4 nanoparticle colloid exhibited a broad, featureless absorbance across the 300–800 nm range without any sharp absorption peaks (Mustafa et al., 2025). This continuous absorption profile is consistent with the optical behavior of iron oxide nanoparticles, which typically display a monotonic increase in absorbance toward the ultraviolet region rather than a defined surface plasmon resonance band (Liang et al., 2024). The brownish-black coloration and broad absorbance of the suspension qualitatively confirm the formation of magnetite nanoparticles. Similar UV–Vis absorption characteristics have been reported for green-synthesized Fe_3O_4 nanoparticles, where broad visible-range absorption arises from intrinsic d–d electronic transitions of Fe^{2+}/Fe^{3+} ions and the absence of plasmonic or quantum confinement effects (Khatun et al., 2022; Das et al., 2025).

When correlated with the FTIR results obtained in this study, the UV–Vis findings further confirm the successful synthesis of Fe_3O_4 nanoparticles capped with biomolecules derived from the lichen extract. Complementary FTIR analysis revealed characteristic vibrational bands associated with organic functional groups adsorbed onto the nanoparticle surface. Prominent absorption bands around 3400 cm^{-1} corresponding to O–H stretching, 1600 cm^{-1} attributed to C=O stretching, and 1050 cm^{-1} assigned to C–O stretching vibrations indicate the presence of polyphenols, flavonoids, and other bioactive compounds that functioned as reducing and stabilizing agents. Similar FTIR features have been reported in previous studies involving plant-mediated synthesis of iron oxide nanoparticles (Mustafa et al., 2025; Eid, 2022). Also, the appearance of a strong absorption band near 580 cm^{-1} confirms the Fe–O stretching vibration, which is a diagnostic feature of magnetite formation (Tiama et al., 2023). The retention of these organic functional groups on the nanoparticle surface supports the role of the lichen extract in providing effective capping, thereby enhancing nanoparticle stability and limiting agglomeration. Collectively, the UV–Vis and FTIR analyses provide robust and complementary evidence for the successful green synthesis of Fe_3O_4 nanoparticles. While UV–Vis spectroscopy elucidates the optical properties and colloidal behavior of the nanoparticles, FTIR spectroscopy reveals the chemical interactions and biomolecular capping mechanisms, thereby validating the efficiency and sustainability of the green synthesis approach (Das et al., 2025).

3.5 Evaluation and Optimization of p-Nitrophenol Adsorption onto Fe_3O_4 Nanoparticles Using Response Surface Methodology

3.5.1 Batch Adsorption Performance of Fe_3O_4 Nanoparticles

Following confirmation of successful Fe_3O_4 nanoparticle synthesis, their adsorption performance toward organic pollutants was evaluated using *p*-nitrophenol (PNP) as a model contaminant. Batch adsorption experiments were conducted to assess the influence of solution pH, contact time, adsorbent dosage, and temperature on PNP removal efficiency. Across the experimental design space, PNP removal efficiencies ranged from approximately 4 % to 55 %, indicating strong dependence on operating conditions. This wide variability underscores the sensitivity of PNP adsorption to physicochemical parameters and aligns with previous reports on nitrophenol adsorption systems (Abd El-Monaem et al., 2023).

3.5.2 Experimental Design and Model Development Using RSM

To optimize adsorption conditions systematically, a 2^4 full-factorial design incorporating four factors (pH, contact time, adsorbent dosage, and temperature) at two levels was employed, resulting in 16 experimental runs. Response Surface Methodology (RSM) was used to develop a predictive model for PNP removal efficiency.

3.5.3 Statistical Validation of the RSM Model

Table 1 presents the analysis of variance (ANOVA) for the factorial model.

Table 1. ANOVA for the factorial model describing PNP adsorption onto Fe_3O_4 nanoparticles

Source	Sum of Squares	df	Mean Square	F-value	p-value
Model	3987.03	12	332.25	37.10	0.0063
A-pH	2342.56	1	2342.56	261.59	0.0005
B-Contact time	86.49	1	86.49	9.66	0.0530
D-Temperature	249.64	1	249.64	27.88	0.0132
AB	277.22	1	277.22	30.96	0.0115
AC	63.20	1	63.20	7.06	0.0766
AD	464.40	1	464.40	51.86	0.0055
BC	7.56	1	7.56	0.8445	0.4259
BD	17.22	1	17.22	1.92	0.2596
ABC	56.25	1	56.25	6.28	0.0872
ABD	392.04	1	392.04	43.78	0.0070
ACD	14.44	1	14.44	1.61	0.2937
BCD	16.00	1	16.00	1.79	0.2737
Residual	26.86	3	8.95		
Cor Total	4013.90	15			

R^2 = 0.9933; Adjusted R^2 = 0.9665; Predicted R^2 = 0.8096; Adeq Precision = 19.3613; Std. Dev. = 2.99; Mean = 31.01; C.V. (%) = 9.65

The ANOVA results demonstrate that the model is statistically significant, with an F-

value of 37.10 and a p-value of 0.0063, confirming significance at the 99 % confidence level.

3.5.4 Model Adequacy and Diagnostic Analysis

The coefficient of determination ($R^2 = 0.9933$) indicates that more than 99 % of the variability in PNP removal is explained by the model. The adjusted R^2 (0.9665) and predicted R^2 (0.8096) are reasonably close, suggesting strong predictive capability without overfitting (Ba-Abbad et al., 2022). Also, the low coefficient of variation (CV = 9.65 %) reflects excellent experimental precision, while the high Adequate Precision value (19.36) indicates a robust signal-to-noise ratio, confirming that the model can reliably navigate the experimental design space.

To further assess model reliability, diagnostic plots comparing predicted and experimental values were examined. The predicted versus actual plot (Fig. 2) shows data points clustering closely around the 45° line, indicating strong agreement between experimental observations and model predictions.

3.5.5 Diagnostic Case Statistics

Table 2 summarizes the diagnostic case statistics for all experimental runs. The small residuals, acceptable leverage values, and low Cook's distance values indicate the absence of influential outliers. Studentized residuals fall within acceptable statistical limits, confirming model robustness and stability. Overall, Table 1 validates the reliability and precision of the RSM model.

3.6 Statistical Interpretation of Factor Effects

The ANOVA results identify solution pH as the most influential factor, with the highest sum of squares and a highly significant p-value ($p = 0.0005$). Increasing pH from acidic to alkaline conditions enhances PNP adsorption, likely due to deprotonation of PNP into its phenolate form, which exhibits stronger electrostatic interaction with Fe_3O_4 surfaces (Kalantari et al., 2024). Temperature also exerts a significant positive effect ($p = 0.0132$), suggesting an endothermic adsorption process. Contact time shows a marginal effect ($p \approx 0.053$), indicating that extended interaction improves adsorption up to near-equilibrium conditions.

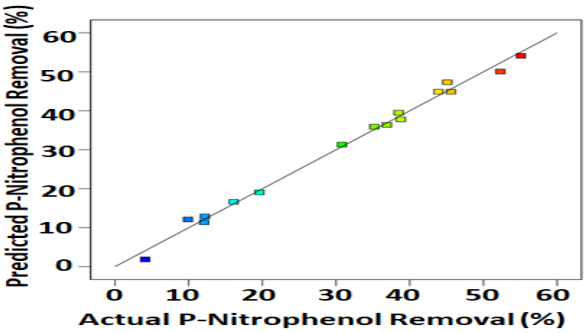

Fig. 2: Predicted vs. Actual PNP Removal

Although adsorbent dosage does not appear as a dominant main effect, its influence manifests through interaction terms. Significant interaction effects—including pH × contact time ($p = 0.0115$), pH × temperature ($p = 0.0055$), and the three-factor interaction pH × contact time × temperature ($p = 0.0070$)—highlight synergistic relationships among operating variables. These interactions indicate that optimal adsorption arises from coordinated tuning of multiple parameters rather than isolated factor adjustment (Aboelfetoh, 2025).

3.7 Optimization of Adsorption Conditions and Practical Implications

Using the validated RSM model, numerical optimization was performed to maximize PNP removal efficiency and the results obtained are summarized in Table 3.

The optimum conditions—pH 8.0, temperature 60 °C, contact time 180 min, and adsorbent dosage 4 g L^{-1}—yielded a predicted PNP removal of 74.93 %, with a desirability value of 1.0. Experimental validation confirmed removal efficiencies in the mid-70 % range, representing a substantial improvement over non-optimized conditions.

Table 2. Diagnostic statistics for PNP adsorption onto Fe_3O_4 nanoparticles

Run Order	Actual Value	Predicted Value	Residual	Leverage	Internally Studentized Residuals	Externally Studentized Residuals	Cook's Distance	Influence on Fitted Value DFFITS	Standard Order
1	30.80	31.32	-0.5250	0.813	-0.405	-0.340	0.055	-0.708	14
2	12.10	11.40	0.7000	0.813	0.540	0.464	0.097	0.966	5
3	52.30	50.08	2.22	0.813	1.717	10.695	0.983	22.263(1)	6
4	35.20	35.90	-0.7000	0.813	-0.540	-0.464	0.097	-0.966	4
5	16.10	16.63	-0.5250	0.813	-0.405	-0.340	0.055	-0.708	15
6	55.10	54.10	1.00	0.813	0.772	0.704	0.199	1.465	16
7	45.10	47.33	-2.23	0.813	-1.717	-10.695	0.983	-22.263(1)	2
8	4.10	1.87	2.23	0.813	1.717	10.695	0.983	22.263(1)	7
9	9.90	12.12	-2.22	0.813	-1.717	-10.695	0.983	-22.263(1)	3
10	45.60	44.90	0.7000	0.813	0.540	0.464	0.097	0.966	8
11	43.90	44.90	-1.00	0.813	-0.772	-0.704	0.199	-1.465	12
12	36.90	36.38	0.5250	0.813	0.405	0.340	0.055	0.708	10
13	12.20	12.90	-0.7000	0.813	-0.540	-0.464	0.097	-0.966	1
14	38.80	37.80	1.0000	0.813	0.772	0.704	0.199	1.465	13
15	19.60	19.08	0.5250	0.813	0.405	0.340	0.055	0.708	11
16	38.50	39.50	-1.0000	0.813	-0.772	-0.704	0.199	-1.465	9

Table 3. Optimized conditions for maximum PNP adsorption onto Fe_3O_4 nanoparticles

	pH	Temperature (°C)	Contact Time (minutes)	Adsorbent Dosage (g/L)	Chlorophenol Removal (%)	Desirability
Fe_3O_4NPs	8	60	180	4	74.925	1.000

These findings emphasize the effectiveness of RSM in enhancing adsorption performance and suggest that Fe_3O_4 nanoparticles are viable candidates for PNP remediation. The positive temperature effect further implies endothermic adsorption behavior, consistent with thermodynamic expectations (Bbumba et al., 2024).

3.8 Adsorption Isotherm Studies

3.8.1 Langmuir Isotherm

The Langmuir model assumes monolayer adsorption onto a homogeneous surface with finite identical sites. Fig. 3 shows the Langmuir isotherm for the adsorption process while values calculated from the plot for the Langmuir parameters are provided in Table 4.

The results obtained indicated that the separation factor R^L (0.095 at C_0 = 50 mg L^{-1}) (Table 4) lies between 0 and 1, confirming favorable adsorption. These results indicate predominantly monolayer adsorption of PNP onto Fe_3O_4 nanoparticles.

3.8.2 Freundlich Isotherm

The linear Langmuir plot (Fig. 3) yielded an excellent correlation (R^2 = 0.9942), with a maximum adsorption capacity (Q_{max}) of 49.75 mg g^{-1} and a Langmuir constant (b) of 0.209 L mg^{-1}.

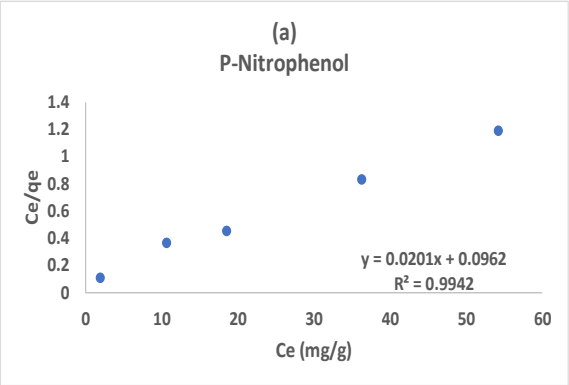

Fig. 3: Langmuir Isotherm (Effect of liquid phase on the fraction of P-Nitrophenol removed from Aqueous medium)

Table 4: Langmuir, Freundlich, and Temkin isotherm parameters for PNP adsorption onto Fe_3O_4 nanoparticles

5

Isotherm	Parameter	Value
Langmuir	Q_e (mg/g)	49.75
	b (L/mg)	0.209
	R^2	0.9942
	R_L (at Co=50 mg/L)	0.095 (favorable)
Freundlich	K_F	3.226
	n (dimensionless)	3.432
	R^2	0.9544
Temkin	K4 (L/mg)	3.781
	B (J/mol)	8.711
	R^2	0.9480

Fig. 4 shows the Freundlich isotherm for the adsorption isotherms. Parameters obtained from the plots were recorded in Table 4

The Freundlich model, which assumes heterogeneous surface energies, also provided a reasonable fit (R^2 = 0.9544). The Freundlich constant K_F = 3.226 and exponent n = 3.432 (1/n = 0.291) indicate favorable adsorption intensity and strong affinity at low concentrations. However, the slightly lower R^2 compared to Langmuir suggests that heterogeneity plays a secondary role in this system.

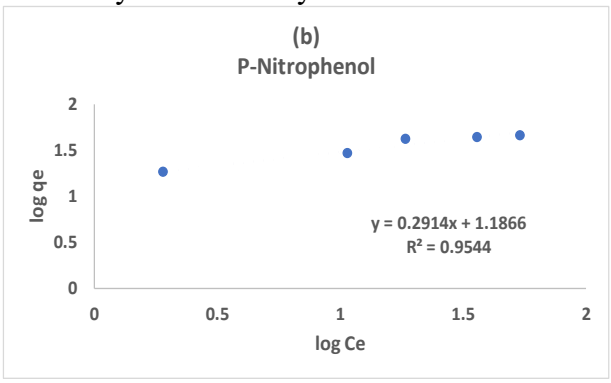

Fig. 4: Freundlich Isotherm (Effect of liquid phase on the fraction of P-Nitrophenol removed

3.8.3 Temkin Isotherm

Also, the Temkin isotherm obtained from the experimental data is shown in Fig. 5 while the Temkin adsorption parameters are contained in Table 4.

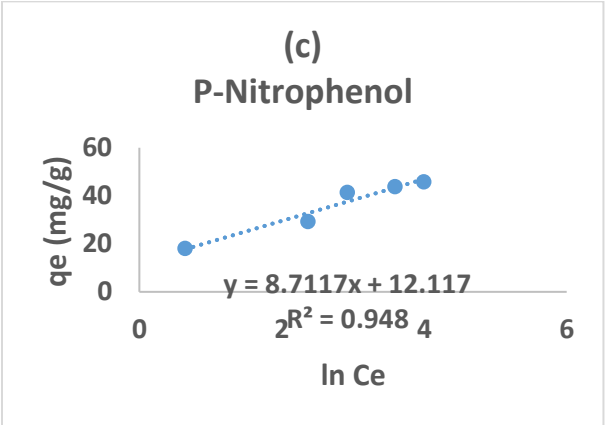

Fig. 5: Temkin Isotherm (Effect of liquid phase on the fraction of P-Nitrophenol removed

The Temkin model yielded an R^2 of 0.9480, indicating moderate agreement. The Temkin constants (β = 8.711 J mol^{-1}, K_T = 3.781 L mg^{-1}) suggest the presence of adsorbate–adsorbent interactions, though these interactions are not the dominant controlling mechanism.

3.9 Comparative Evaluation of Isotherm Models

Comparison of correlation coefficients reveals that the Langmuir model best describes PNP adsorption onto Fe_3O_4 nanoparticles, followed by Freundlich and Temkin. This indicates that adsorption predominantly occurs via monolayer coverage on relatively uniform surface sites. While Freundlich and Temkin models capture aspects of surface heterogeneity and interaction effects, their lower R^2 values confirm that Langmuir assumptions are more appropriate for this system. Consequently, Fe_3O_4 nanoparticles exhibit a well-defined adsorption capacity, making Langmuir modeling suitable for process design and scale-up applications

4. 0 Conclusions

Green Synthesis Validated through the use of SEM, TEM, UV-Vis and FTIR spectra and Adsorption studies confirmed successful Fe_3O_4 formation with biomolecular capping. Adsorption Efficacy Demonstrated maximum PNP removal of 74.93 % under optimized conditions highlights Fe_3O_4's potential for water purification. Model Fit and Significance. The statistical model ($R^2 > 0.99$) reliably describes system behavior, with low CV and high Adequate Precision ensuring experimental robustness. Synergistic interactions observed significant interaction among the tested conditions (pH × temperature, pH × contact time) showed complex dynamics affecting removal performance. Fe_3O_4 nanoparticles effectively adsorbed para nitrophenol (PNPS) under studied conditions, achieving a monolayer adsorption capacity of 49.75 mg/g. The Langmuir model's dominance confirms that adsorption is favourable, spontaneous, and likely limited by saturation of uniform surface sites. R^L values < 1 across the concentration range reinforce the efficiency of adsorption, especially in dilute wastewater scenarios.

5.0 References

Abd El-Monaem, E. M., Eltaweil, A. S., El-Subruiti, G. M., Mohy-Eldin, M. S., & Omer, A. M. (2023). Adsorption of nitrophenol onto a novel Fe_3O_4-κ-carrageenan/MIL-125(Ti) composite: Process optimization, isotherms, kinetics, and mechanism. *Environmental Science and Pollution Research*, 30, 17, pp. 49301–49313. https://doi.org/10.1007/s11356-023-25678-2

Aboelfetoh, E. F. (2025). One-step hydrothermal synthesis of magnetically separable rGO-supported Fe_3O_4 and Ag nanoparticles for adsorption and reduction of organic pollutants. *Scientific Reports*, 15, 12170. https://www.nature.com/articles/s41598-025-121709

Adeyemi, O. T., & Adedeji, T. A. (2020). Evaluation of phytochemical constituents and antioxidant potentials of lichens in Nigeria. *Journal of Applied Sciences and Environmental Management,* 24, 4, pp. 699–704. https://doi.org/10.4314/jasem.v24i4.26

Alamier, W. M., El-Moselhy, M. M., Bakry, A. M., Hasan, N., & Alamri, A. A. (2022). Biogenic synthesis of zero valent Fe/magnetite Fe_3O_4 nanoparticles using *Caralluma acutangula* and application for methylene blue dye degradation under UV light irradiation. *Crystals,* 12, 11, 1510. https://doi.org/10.3390/cryst12111510.

Awad, M. A., Mohamed, R. M., & El-Shamy, A. M. (2020). Photocatalytic activity of TiO_2 nanoparticles prepared by green synthesis method using different plant extracts. *Journal of Photochemistry and Photobiology B: Biology, 204*, 111792. https://doi.org/10.1016/j.jphotobiol.2020.111792

Azizi, A., Mahmoudi, E., & Sadeghi, M. (2020). Green synthesis of Fe_3O_4 nanoparticles and its application in preparation of Fe_3O_4/cellulose magnetic nanocomposite: A suitable proposal for drug delivery systems.

Journal of Inorganic and Organometallic Polymers and Materials, 30, 10, pp. 3844–3852. https://doi.org/10.1007/s10904-020-01500-1.

Bassim, S., Mageed, A. K., AbdulRazak, A. A., & Majdi, H. S. (2022). Green synthesis of Fe_3O_4 nanoparticles and its applications in wastewater treatment. *Inorganics,* 10, 12, 260. https://doi.org/10.3390/inorganics10120260.

Benmaati A, Boukoussa B, Hadjadj Aoul R, Hachemaoui M, Kerbadou RM, Habib Zahmani H, Hacini S (2022). Insights into catalytic reduction of organic pollutants catalyzed by nanoparticles supported on zeolite clinoptilolite. *Silicon,* 14, pp. 8831–8843. https://doi. org/10.1007/s12633-022-01671-1

Bharathi, D., Rajalakshmi, G., & Anuja, R. (2018). Comparative study of iron oxide nanoparticles synthesized from various biological sources and their antibacterial activity. *Biochemistry and Biophysics Reports,* 14, pp. 313–319. https://doi.org/10.10 16/j.bbrep.2018.05.005.

Chakraborty, S., Das, B., Saha, A., & Ghosh, S. (2023). Green synthesis of iron oxide nanoparticles and their potential environmental applications: A review. Environmental Nanotechnology, Monitoring & Management, 20, 100776. https://doi.org/10.1016/j.enmm.2023.100776

Chen, X., Li, Y., Pan, X., Cortie, D., Huang, X., & Yi, Z. (2021). Photocatalytic degradation of organic pollutants using TiO_2- and ZnO-based nanomaterials. *Environmental Science and Pollution Research,* 28, 4, 4475–4496. https://doi.org/10.1007/s11356-020-11045-6

Das, T. K., & Das, N. C. (2022). Mussel-inspired green synthesis of silver nanoparticles-decorated halloysite nanotube using dopamine: Characterization and evaluation of its catalytic activity. *Applied Nanoscience,* 12, 1, pp. 173–186. https://doi.org/10.1007/s13204-018-0658-3

Das, T., Kaur, M., Kaur, N., Bhowmik, P. K., Han, H., Sohal, H. S., & Husain, F. M. (2025). Greener and magnetic Fe_3O_4 nanoparticles as a recyclable catalyst for Knoevenagel condensation and degradation of industrial Congo red dye. *Green Processing and Synthesis,* 14, 1, https://doi.org/10.1515/gps-2024-0257.

Debnath, S. C., Das, M. P., & Mukherjee, A. (2016). Biosynthesis of gold nanoparticles using Sticta sp. lichen extract and evaluation of their catalytic and antibacterial activity. *Materials Letters,* 185, pp. 215–218. https://doi.org/10.1016/j.matlet.2016.08.013

Devi, T. P., Sahu, P. S., Kakati, D. K., & Sarma, B. K. (2021). Plant-based synthesis of iron oxide nanoparticles: A review of recent trends and advancements. *Journal of Environmental Chemical Engineering*, 9, 4, 105549. https://doi.org/10.1016/j.jece.2021.105549

Du, J. (2023). Adsorption thermodynamics and kinetics of nanomaterials: Theory and experimental insight into nano-effect. *The Journal of Chemical Physics,* 159, 23, 234106. https://doi.org/10.1063/5.0177329

Ebelegi, A. N., Ayawei, N., & Wankasi, D. (2020). Interpretation of adsorption thermodynamics and kinetics. *Open Journal of Physical Chemistry, 10*(3), 166–182. https://doi.org/10.4236/ojpc.2020.103010

Eddy, N. O., Odiongenyi, A. O., Garg, R., Ukpe, R. A., Garg, R., El Nemr, A., Ngwu, C. M., & Okop, I. J. (2023). Quantum and experimental investigation of the application of *Crassostrea gasar* (mangrove oyster) shell–based CaO nanoparticles as adsorbent and photocatalyst for the removal of crystal violet dye from aqueous solution. *Environmental Science and Pollution Research*, *30*(23), 64036–64057.

https://doi.org/10.1007/s11356-023-26715-x

El-Sayed, M., & Hassan, A. (2023). *Biosensing and anti-inflammatory effects of silver, copper and iron nanoparticles from Catharanthus roseus*. Bulletin of the National Research Centre, 47, 1, 358. https://bjbas.springeropen.com/articles/10.1186/s43088-023-00358-9

Gao, Y., Liu, D., Huang, C., & Zhao, Z. (2022). Green synthesis of metal oxide nanoparticles and their biomedical applications: Recent advances and future perspectives. Colloids and Surfaces B: Biointerfaces, 210, 112249. https://doi .org/10.1016/j.colsurfb.2021.112249

Gogoi, S., & Dutta, R. K. (2020). *Nanofibers in water purification: Challenges and advancements*. Materials Today: Proceedings, 26, 2, pp. 1948–1955.

Golabiazar, R. (2023). Green synthesis and characterization of magnetite nanoparticles (Fe_3O_4 NPs) using Qazwan seeds extract as antimicrobial agent. *Iranian Journal of Chemistry and Chemical Engineering, 42*(9), 2745–2756. https://doi.org/10.30492/ijcce.2023.561234.5552.

Gupta, S. S., & Nayak, A. (2018). Application of nanomaterials in water treatment: A review. *Environmental Nanotechnology, Monitoring & Management, 9*, 23–30. https://doi.org/10.1016/j.enmm.2017.12.003

Khamizov, R. K. (2020). A pseudo-second order kinetic equation for sorption processes. *Russian Journal of Physical Chemistry A,* 94*, 1, pp,* 171–176. https://doi.org/10.1134/S0036024420010148

Khatun, R., Al Mamun, M. S., Islam, S., Khatun, N., Hakim, M., Hossain, M. S., Dhar, P. K., & Barai, H. R. (2022). Phytochemical-assisted synthesis of Fe_3O_4 nanoparticles and evaluation of their catalytic activity. *Micromachines,* 13, 12, 2077. https://doi.org/10.3390/mi13122077

Khatun, R., Al Mamun, M. S., Islam, S., Khatun, N., Hakim, M., Hossain, M. S., Dhar, P. K., & Barai, H. R. (2022). Phytochemical-assisted synthesis of Fe_3O_4 nanoparticles and evaluation of their catalytic activity. *Micromachines,* 13, 12, 2077. https://doi.org/10.3390/mi13122077

Khoirotin, K., Faaizatunnisa, N., & Munasir, M. (2023). Green synthesis of Fe_3O_4 nanoparticles using green betel leaf (*Piper betle*) extract for methylene blue adsorption. *Natural and Life Sciences Communications*, 22*(, 3,* e2023042. https://doi.org/10.12982/NLSC.2023.042

Kiwumulo, H. F., Muwonge, H., Ibingira, C., Lubwama, M., Kirabira, J. B., & Ssekitoleko, R. T. (2022). Green synthesis and characterization of iron-oxide nanoparticles using *Moringa oleifera*: A potential protocol for use in low and middle income countries. *BMC Research Notes*, 15, 149. https://doi.org/10.1186/s13104-022-06039-7

Kumar, R., Umar, A., Kumar, G., Koo, B., & Kim, S. H. (2018). Photocatalytic degradation of environmental pollutants using nanocatalysts: A review. *Environmental Research,* 164*,* pp. 420–435. https://doi.org/10.1016/j.envres.2018.03.011

Li, N., Zhou, Q., Wang, H., & Zhang, M. (2020). Advances in nano-enabled membrane technologies for water purification. *Journal of Membrane Science,* 611*,* 118281. https://doi.org/10.1016/j.memsci.2020.118281

Li, Q., Lv, C., Xia, X., Peng, C., Yang, Y., Guo, F., & Zhang, J. (2022). *Separation/degradation behavior and mechanism for cationic/anionic dyes by Ag-functionalized Fe_3O_4-PDA core-shell adsorbents*. *Frontiers of Environmental Science & Engineering*, 16, 138, https://doi.org/10.1007/s11783-022-1572-1

Li, X., Elliott, D. W., & Zhang, W. X. (2006). Zero-valent iron nanoparticles for abatement of environmental pollutants: Materials and engineering aspects. *Critical Reviews in Solid State and Materials Sciences,* 31, 4, pp. 111–122. https://doi.org/10.1080/10408430600912438.

Liang, Y., Jiang, L., Xu, S., Ju, W., Tao, Z., Yang, Y., Peng, X., & Wei, G. (2024). Synthesis and characterization of Fe_3O_4 nanoparticles prepared by solvothermal method. *Journal of Materials Engineering and Performance, 33*, 6804–6815. https://doi.org/10.1007/s11665-023-08431-1

Moosav, S.; Lai, C.W.; Gan, S.; Zamiri, G.; Pivehzhani, O.A.; Johan, M.R. Application of Efficient Magnetic Particles and Activated Carbon for Dye Removal from Wastewater. *ACS Omega* 2020, 5, pp. 20684–20697.

Mustafa, A., Ali, U., Mukarama, M., Iqbal, A., Qayyum, M., Haq, I. U., & Islam, F. (2025). Synthesis and characterization of Fe_3O_4 nanoparticles by sol-gel method using water as a solvent. *Advances in Nanoparticles,* 14, 1, pp. 1–11. https://doi.org/10.4236/anp.2025.141001

Nikou, M., Samadi-Maybodi, A., & Yasrebi, K. (2025). Modeling process of reduction of 4-nitrophenol pollutant from aqueous medium by Fe_3O_4@SiO_2@Zr-MOF-NH_2/Ag nanocatalyst and fuzzy logic. *Arabian Journal for Science and Engineering*. https://doi.org/10.1007/s13369-025-10250-6

Oladoja, N. A. (2016). A critical review of the applicability of Avrami fractional kinetic equation in adsorption-based water treatment studies. *Desalination and Water Treatment,* 57, 34, pp. 15813–15825. https://doi.org/10.1080/19443994.2015.1076355

Osman, H., Uğurlu, M., Vaizoğullar, A. İ., Atasoy, M., & Chaudhary, A. J. (2024). Statistical modeling and optimization of heavy metals (Pb and Cd) adsorption from aqueous solution by synthesis of Fe_3O_4/SiO_2/PAM. *Polymer Bulletin,* 81, pp. 14513–14545. https://doi.org/10.1007/s00289-024-05404-9

Rahaman, M. S., Vecitis, C. D., & Elimelech, M. (2021). Emerging nanotechnology-based approaches for water treatment. *Environmental Science & Technology, 55, 4, pp.* 2038–2056. https://doi.org/10.1021/acs.est.0c07721

Rattan, R. K., Chauhan, R., Sharma, A., & Mehta, S. K. (2021). Lichens as a potential bioresource for the green synthesis of nanoparticles: A comprehensive review. *Environmental Nanotechnology, Monitoring & Management,* 16, 100538. https://doi.org/10.1016/j.enmm.2021.100538

Riyanti, F., Nursari, F., Ahadito, B. R., Hanum, L., Eliza, & Hariani, P. L. (2023). Green synthesis of Fe_3O_4 magnetic nanoparticle by *Moringa oleifera* leaf extract for photocatalytic degradation of Congo red dye. *EAI Endorsed Transactions on Energy Web*, 10, 3, e2347962. https://doi.org/10.4108/eai.3-11-2023.2347962

Rodriguez Mejía, Y., & Bogireddy, N. K. R. (2022). Reduction of 4-nitrophenol using green-fabricated metal nanoparticles. *RSC Advances, 12*, 18661–18675. https://doi.org/10.1039/D2RA02663E

Rukmini, R. (2020). Phytochemical screening of green betel (*Piper betle*) leaves and their role in nanoparticle synthesis. *Journal of Medicinal Plants Research*, 14, 5, pp. 210–216.

Safarkar, R., Zarei, A. A., & Shamsipur, M. (2020). Biosynthesis of silver nanoparticles using Ramalina sinensis lichen extract and evaluation of their antibacterial activity. *Materials Science and Engineering: C, 113*,

110975. https://doi.org/10.1016/j.msec.2020.110975

Samghouli, N., Bencheikh, I., Azoulay, K., Jansson, S., & El Hajjaji, S. (2025). *Mechanistic and reactional activation study of carbons destined for emerging pharmaceutical pollutant adsorption*. Environmental Monitoring and Assessment, 197, 259. https://doi.org/10.1007/s10661-025-13685-4

Shaikh, S., Naz, S., Ahamed, M., & Ahmad, J. (2022). Plant-extract-mediated iron oxide nanoparticles: A review on their synthesis, characterization, and biomedical applications. Journal of Drug Delivery Science and Technology, 71, 103263. https://doi.org/10.1016/j.jddst.2022.103263

Sharma, P., & Verma, R. (2025). *Catharanthus roseus-mediated iron oxide nanoparticles demonstrate enhanced antibacterial, antioxidant, and anti-diabetic properties*. Journal of Applied Biology & Biotechnology, 13, 1, pp. 45–52. https://jabonline.in/admin/php/uploads/1342_pdf.pdf

Singh, J., Dutta, T., Kim, K. H., Rawat, M., Samddar, P., & Kumar, P. (2018). 'Green' synthesis of metals and their oxide nanoparticles: Applications for environmental remediation. *Journal of Nanobiotechnology, 16*, 84. https://doi.org/10.1186/s12951-018-0408-4

Temkin, M., & Pyzhev, V. (1940). Kinetics of ammonia synthesis on promoted iron catalysts. *Acta Physicochimica URSS*, 12, pp. 327–356.

Tran, H. N. (2023). Applying linear forms of pseudo-second-order kinetic model for feasibly identifying errors in the initial periods of time-dependent adsorption datasets. *Water,* 15, 6, 1231. https://doi.org/10.3390/w15061231

Trujillo Hernandez, J. S., Aragón-Muriel, A., Corrales Quintero, W., Castro Velásquez, J. C., Salazar-Camacho, N. A., Pérez Alcázar, G. A., & Tabares, J. A. (2022). Characterization of Fe_3O_4 nanoparticles for applications in catalytic activity in the adsorption/degradation of methylene blue and esterification. *Molecules,* 27, 24, 8976. https://doi.org/10.3390/molecules27248976

.Tumbelaka, R. M., Istiqomah, N. I., Mabarroh, N., & Suharyadi, E. (2022). Green synthesis of Fe_3O_4/TiO_2 nanoparticles using extracts of *Moringa oleifera*: Microstructural and optical properties. *Solid State Phenomena*, *332*, pp.91–99. https://doi.org/10.4028/p-oi81sf

Umar, A., Zafar, M., Rahman, M. M., & Akhtar, M. S. (2024). Recent progress on the green synthesis and environmental applications of metal oxide nanoparticles: A comprehensive review. *Journal of Industrial and Engineering Chemistry*, 123, pp. 1–22. https://doi.org/10.1016/j.jiec.2023.11.027

Varun, R., M. (2025). Removal of Phenol derivatives from water systems with the use of silver nanoparticles. *Chemical Engineering Journal,* 23, pp. 1-22. https://doi.org /10.26434/chemrxiv-2025-gzq66.

Vigdorowitsch, M., Pchelintsev, A. N., & Tsygankova, L. E. (2021). Analytical continuation within the Freundlich adsorption model. *Processes,* 9, 7, 1251. https://doi.org/10.3390/pr9071251

Vigdorowitsch, M., Pchelintsev, A., Tsygankova, L., & Tanygina, E. (2021). Freundlich isotherm: An adsorption model complete framework. *Applied Sciences,* 11(17), 8078. https://doi.org/10.3390/app11178078

Vimala, K., Sundarraj, S., Paulpandi, M., Vengatesan, S., & Kannan, S. (2014). Green synthesized doxorubicin loaded zinc oxide nanoparticles regulate Bax and Bcl-2 expression in breast and colon carcinoma. *Process Biochemistry, 49*(1), 160–172. https://doi.org/10.1016/j.procbio.2013.10.006

Vu, A. N., Le, H. N. T., Phan, T. B., & Le, H. V. (2023). Facile hydrothermal synthesis of Ag/Fe_3O_4/cellulose nanocomposite as highly active catalyst for 4-nitrophenol and organic dye reduction. *Polymers,* 15, 16, 3373. https://doi.org/10.3390/polym15163373

Wei, Y., Zhang, Y., Wang, Y., Tang, Z., & Li, J. (2016). Green synthesis of Fe_3O_4 nanoparticles using seaweed extract. *Applied Surface Science,* 384, pp. 122–130. https://doi.org/10.1016/j.apsusc.2016.05.104

Yahya, A. A., Rashid, K. T., Ghadhban, M. Y., Mousa, N. E., Majdi, H. S., Salih, I. K., & Alsalhy, Q. F. (2021). Removal of 4-nitrophenol from aqueous solution by using polyphenylsulfone-based blend membranes: Characterization and performance. *Membranes,* 11, 3, 171. https://doi.org/10.3390/membranes11030171

Yahya, G., Pérez, A. P., Mendoza, M. B., Parisi, E., Moreno, D. F., Artés, M. H., Gallego, C., & Aldea, M. (2021). Stress granules display bistable dynamics modulated by Cdk. *Journal of Cell Biology*, 220, 3, , e202005102. https://doi.org/10.1083/jcb.202005102

Yan, P.; He, M.; Chen, B.; Hu, B. (2015). Restricted accessed nanoparticles for direct magnetic solid phase extraction of trace metal ions from human fluids followed by inductively coupled plasma mass spectrometry detection. Analyst,140, pp. 4298–4306.

Yang, W., & He, J. (2022). Recent advances in nanocatalysts for environmental remediation. *Chemical Engineering Journal, 430*, 132728. https://doi.org/10.1016/j.cej.2021.132728

Yıldızel, S. A., Karalar, M., Aksoylu, C., Althaqafi, E., Beskopylny, A. N., Stel'makh, S. A., Shcherban', E. M., Umiye, O. A., & Özkılıç, Y. O. (2025). Optimization of concrete with human hair using experimental study and artificial neural network via response surface methodology and ANOVA. *Scientific Reports,* 15, 12782. https://doi.org/10.1038/s41598-025-12782-1

Zhao, Y., Zhang, J., Wang, X., & Wang, C. (2019). Recent advances in nanosensors for environmental pollutant detection and monitoring. *Environmental Science: Nano,* 6, 1, pp. 63–85. https://doi.org/10.1039/C8EN00724F

Zhou, C., Wang, Q., Zhang, Y., Li, X., & Wu, W. (2020). Catalytic properties and environmental applications of nanocatalysts. *Journal of Environmental Chemical Engineering,* 8, 4, 103883. https://doi.org/10.1016/j.jece. 2020.103883

Declaration

Consent for publication

Not Applicable

Availability of data and materials

The publisher has the right to make the data public

Ethical Considerations

Not applicable

Competing interest

The authors report no conflict or competing interest

Funding

No funding

Author Contributions

A.A. conceived the study, carried out the green synthesis, and performed adsorption experiments. C.N.N. conducted characterization analyses and data validation. K.I.O. handled statistical modeling and RSM optimization. I.H. supported laboratory work and literature review. M.A.S. supervised the research, interpreted results, and finalized the manuscript.